Radiochim. Acta **93**, 225–232 (2005)


# Characterization of $Sr^{2+}$ uptake on natural minerals of kaolinite and magnesite using XRPD, SEM/EDS, XPS, and DRIFT

By T. Shahwan[1,*] and H. N. Erten[2]

[1] Department of Chemistry, Izmir Institute of Technology, 35430 Urla, Izmir, Turkey
[2] Department of Chemistry, Bilkent University, 06800 Bilkent, Ankara, Turkey

(Received August 26, 2004; accepted in revised form October 26, 2004)

$Sr^{2+}$ / *Kaolinite* / *Magnesite*

**Summary.** The sorption behavior of $Sr^{2+}$ ions on natural minerals rich in kaolinite and magnesite was studied using SEM/EDS, XPS, XRPD, AAS/AES and DRIFT techniques. Quantitative analysis of the XPS data shows that magnesite is more effective in $Sr^{2+}$ uptake than kaolinite. DRIFT spectra and XRPD patterns indicate that the structures of both minerals were not affected upon $Sr^{2+}$ sorption. Intercalation of DMSO in kaolinite lamellae aiming at increasing the interlayer space did not significantly enhance the sorption capacity of the clay towards $Sr^{2+}$ probably due to the lack of a negative charge on the accessible sites. EDS mapping indicated that while the sorbed Sr is equally distributed on surface of natural kaolinite, it was associated – to a larger extent – with the regions richer in Mg in the case of natural magnesite. Comparing the uptake mechanisms of natural magnesite with that of pure $MgCO_3$, it was seen that while natural magnesite sorbed $Sr^{2+}$ mainly through an ion exchange type mechanism, the formation of $SrCO_3$ coprecipitate was detected on the surface of the $MgCO_3$ at higher loadings.

## Introduction

Disposal of radionuclides that are potentially harmful to the biological environment into underground repositories requires a thorough assessment of radiological hazards that might arise from the long term storage of the radioactive waste in geological formations. Soil forms a natural barrier against the migration of radionuclides into the bioenvironment and therefore studies regarding interactions between various radionuclides and soil fractions are essential in establishing an understanding of the extent of retardation of radionuclides migration.

From radioactive waste management view point, $^{90}Sr$ ($t_{1/2} = 29.1$ y) possesses a particular importance due to its long half life and high yield (5.77%) during fission [1]. Various studies have been carried out to examine different aspects of the sorption behavior of Sr on a variety of solid materials [2–13]. Whereas the sorption behavior of $Sr^{2+}$ on kaolinite was investigated in a limited number of studies [14–17], our literature survey did not yield information regarding the uptake of $Sr^{2+}$ by magnesite, although it is one of the most important carbonates on Earth's crust.

In general, the sorption reactions on kaolinite are expected to occur rapidly with ion exchange reported to be the retention mechanism taking place mostly at the surface and edge positions of the clay. This stems from the structural properties of kaolinite which possesses a relatively tight interlayer structure held by H-bonds. This makes sorption by interlayer sites improbable and as a result limits the sorption capacity of kaolinite compared with the sorption capacity of other expandable clays like montmorillonite. It is reported that the cation exchange capacity of kaolinite is about one-tenth of that of montmorillonite [18]. In a detailed study using SEM/EDS, XANES and EXAFS techniques, it was observed that the dominant exchange sites in kaolinite have an octahedral geometry and that $Sr^{2+}$ binds to the kaolinite surface by exchanging into the relatively abundant octahedral sites found near the surface and – less commonly – at the edges of the clay [15].

In this study, the sorption of $Sr^{2+}$ on two natural soil fractions originating from Turkey was investigated. The soil fractions used in this work were obtained from natural deposits and were rich in kaolinite and magnesite. The surface sensitive technique of X-ray photoelectron spectroscopy (XPS) was used to reveal the amount of Sr that was sorbed by each soil fraction and identify the quantities of various ions – originally present in the soil structure – prior to and following $Sr^{2+}$ sorption. The amount of $Sr^{2+}$ remaining in solution at the end of sorption was also measured using atomic absorption spectroscopy (AAS). Diffuse reflectance infrared spectroscopy (DRIFT) and powder X-ray diffraction (XRPD) were used to characterize the natural minerals and elucidate any structural change occurring in the solid matrices as a result of sorption. Back scattered electron images were recorded and elemental contents of the minerals were analyzed using scanning electron microscope-energy dispersive X-ray spectroscopy (SEM/EDS).

## Experimental

### Sorption experiments

The natural soil fractions were obtained from the Turkish General Directorate of Mineral Research and Exploration

*Author for correspondence (E-mail: talalshahwan@iyte.edu.tr).

(MTA). The samples were dry sieved and the particle size of the samples used in the experiments were $< 38\ \mu m$. Batch method was used throughout the study. The sorption experiments were carried out by shaking 100.0 mL aliquots of $1.0 \times 10^{-2}$, $1.0 \times 10^{-4}$, and $1.0 \times 10^{-6}$ M of $SrCl_2$ solutions with 1.0 g of each of the mineral fractions for 48 hours using a magnetic stirrer. The samples were then filtrated and dried overnight at 90 °C. Throughout this work, no attempt was made to adjust the pH or fix it to a certain value, as we were attempting to mimic the situation in the natural systems which allows for pH fluctuations in the course of interaction between aqueous solutions of metals and the soil fractions. During the sorption experiments of $Sr^{2+}$ on kaolinite, the pH range was 5.7–7.3. In the case of sorption on natural magnesite and pure $MgCO_3$, the pH ranges were 8.2–7.6 and 10.5–8.3, respectively. Within the pH of our experiments, the chemical form of Sr in aqueous solution is expected to be $Sr^{2+}$. This element belongs to group II which contains elements of low charge densities, in particular those of higher atomic weight like Sr. At neutral pH values or even in moderately alkaline media, alkaline earth elements show little tendency to hydrolyze, the thing that makes hydroxyl, $SrOH^+$, or hydroxide, $Sr(OH)_2$, specie soluble in aqueous media [19].

The intercalation of dimethylsulfoxide (DMSO) within the kaolinite lamellae was achieved by stirring a suspension composed of 20 g of the clay in 100 ml DMSO for 24 hours at 65 °C. The redundant DMSO was then removed by sedimentation repeated washes with methanol and decanting over a period of 5 days [20].

Flame–atomic absorption/emission spectroscopy (AAS/AES) were used for bulk analysis of the filtrates by using a Thermo Elemental SOLAAR M6 Series atomic absorption spectrometer with air-acetylene flame (or nitrous oxide-acetylene, as in the case of Si analysis) being used as oxidant-fuel.

Diffuse-reflectance (DRIFT) technique was used to record the spectra of the minerals in the middle IR region using a Nicole Magna 550 type instrument. The samples were introduced as powders diluted with KBr and the spectra were recorded in the range 400–4000 $cm^{-1}$. The resolution was 4 $cm^{-1}$ and a total of 32 scans were recorded for each spectrum. The software used to process the results was Omnic 1.3.

The solid samples were sprinkled onto adhesive carbon taps supported by circular metallic disks. The samples were then analyzed using a Philips XL-30S FEG type SEM/EDS instrument. Images of the sample surfaces were recorded at different magnifications with the highest being $\times 80\,000$. EDS elemental analysis was performed at five different points of the surface in order to minimize any possible anomalies arising from the heterogeneous nature of the analyzed surface. EDS mapping was conducted at magnification of $\times 500$ and a voltage of 18 kV under vacuum conditions of $3.5 \times 10^{-5}$ mbar.

The XPS spectra of the mineral samples prior to and following sorption of $Sr^{2+}$ were recorded using a VG Scientific Escascope instrument – located at the interface analysis centre at University of Bristol – with Mg $K_\alpha$ X-rays ($h\nu = 1253.6$ eV) as a source. Wide and regional spectra were recorded with step scans of 40 eV, 30 eV and step sizes of 1.0 and 0.1 eV, respectively. Samples were mounted as freshly ground powders pressed onto adhesive copper tape. Pressure was kept below $1 \times 10^{-8}$ mbar during analysis. C 1*s* line (B.E = 284.8 eV) originating from the adventitious hydrocarbons at the surface of the samples was used as the reference line. Sensitivity corrections were done using Wagner sensitivity factors and quantification was performed *via* a VG Scientific VGS5250 software.

Samples of natural-, and Sr-sorbed mineral fractions were first ground, mounted on rectangular glass holders, then introduced for X-ray diffraction analysis. A Rigaku miniflex X-ray diffractometer was used. The source consisted of unfiltered Cu $K_\alpha$ radiation, generated in a tube operating at 30 kV and 15 mA. Spectra were recorded with 2 theta values ranging from 2 to 60 degrees – depending on the type of the analyzed sample – in steps of 0.02 degree and dwell times of 10 s per step. Analysis was performed at ambient temperature.

## Results and discussion

### Characterization of the natural minerals

The XRPD analysis showed that the natural kaolinite samples were composed of kaolinite and quartz as an impurity (Fig. 1a). In the figure, kaolinite is characterized by the marked 001 and 002 features and the presence of quartz in the sample is evident from the well known 101 and 100 peaks. The XPRD analysis of the natural magnesite samples indicated the presence of some quartz, calcite, and kaolinite in addition to the major $MgCO_3$ component (Fig. 2a). Magnesite is characterized mainly by the 104 reflection in addition to other less intense features as shown in the corresponding figure.

The DRIFT spectra of natural kaolinite and natural magnesite are given in Figs. 3 and 4, respectively. Kaolins can be readily distinguished from other clays by differences in position and relative intensities of their OH stretching bands. The OH stretchings occurring around the 3700–3620 $cm^{-1}$ doublet are characteristic for kaolin clays. The feature near 3700 $cm^{-1}$ lies well separated from those of most other min-

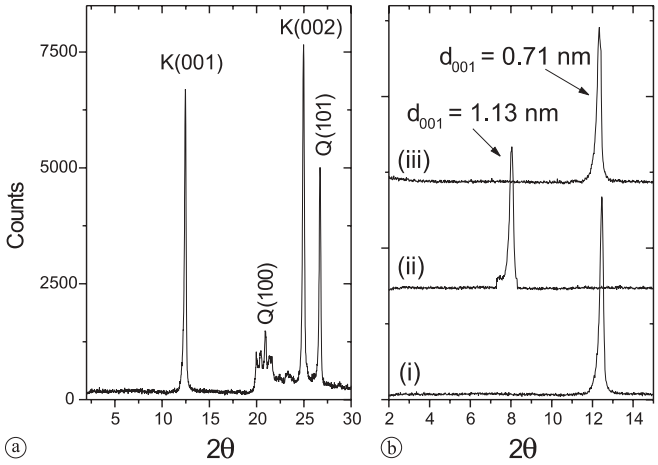


**Fig. 1.** XRPD diagrams of: (**a**) natural kaolinite, (**b**) the $d_{001}$ reflection in (i) natural kaolinite, (ii) DMSO-intercalated kaolinite, (iii) Sr sorbed (DMSO-intercalated) kaolinite. K: kaolinite, Q: quartz.

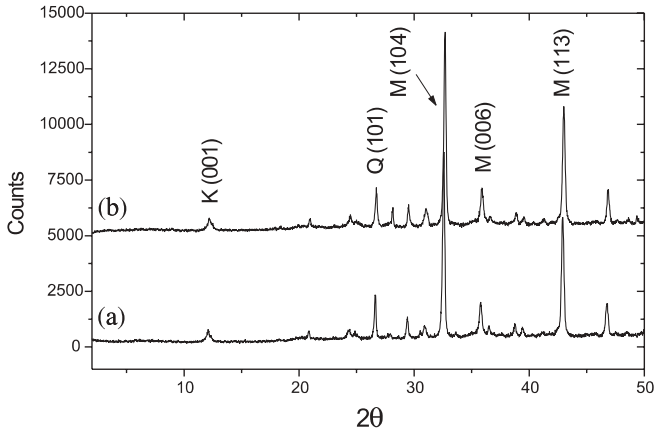


**Fig. 2.** XRPD diagrams of: (a) natural magnesite, (b) Sr-sorbed magnesite ($1.0 \times 10^{-2}$ M). K: kaolinite, Q: quartz, M: magnesite.

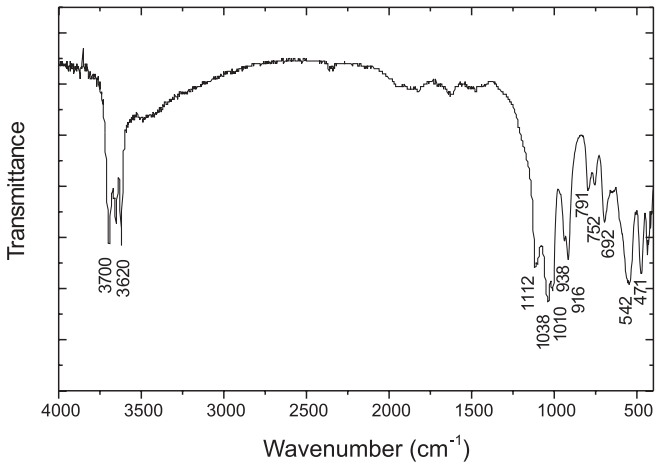


**Fig. 3.** DRIFT spectrum of: kaolinite.

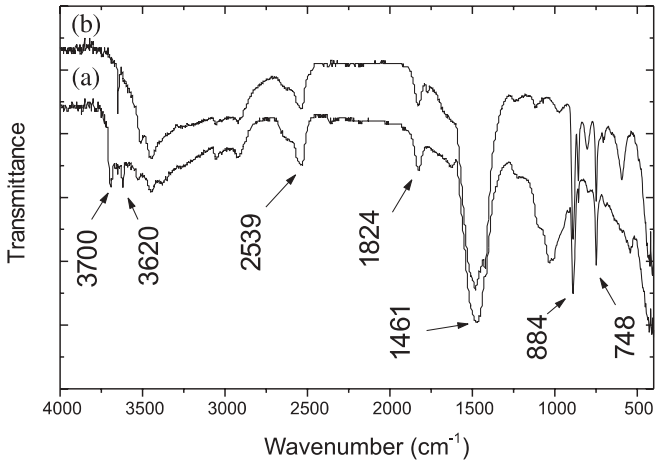


**Fig. 4.** DRIFT spectrum of: (a) natural magnesite, (b) pure $MgCO_3$.

eral bands. The OH deformation bands near 938–916 $cm^{-1}$ are also typical for the kaolin group minerals and arise from vibrations of the inner and inner surface OH groups within the clay matrix [21]. Other features appearing in the spectrum belong to a variety of Al−O and Si−O stretching and bending vibrations [22]. A detailed assignment of all the bands arising in the kaolinite spectrum is given in Table 1.

The DRIFT spectra of natural magnesite and pure $MgCO_3$ are shown in Fig. 4a and b, respectively. The FTIR

**Table 1.** Assignments of the bands appearing in the DRIFT spectrum of natural kaolinite.

| Band Position ($cm^{-1}$) | Vibration Assignment |
|---|---|
| 3700 | Inner surface −OH stretching vibration |
| 3620 | Inner −OH stretching vibration |
| 1112, 1038, 1010 | Si−O bending vibration |
| 938, 918 | Al−OH bending vibration |
| 792, 754 | Si−O−Al compound vibrations |
| 692 | Si−O stretching vibration |
| 540 | Si−O−Al compound vibrations |
| 471, 433 | Si−O vibrations |

spectra of carbonate minerals contains modes arising from out-of-plane bending ($\nu_2$), the asymmetric stretching ($\nu_3$), the in-plane-bending ($\nu_4$), and the combination modes ($\nu_1 + \nu_3$) and ($\nu_1 + \nu_4$). The symmetric stretching mode ($\nu_1$) is usually very weak and hardly detected [23] and its presence is referred to a disorder in the symmetry of carbonate group. Complete assignment of the bands is given in Table 2. The bands arising from the vibrational modes of carbonate in natural magnesite coincide with the bands belonging to pure $MgCO_3$ as shown in the Fig. 2. On the other hand, the bands appearing near 3700 and 3620 $cm^{-1}$ in the spectrum of natural magnesite belong to the kaolinite impurity in the magnesite mineral.

Natural kaolinite and magnesite samples were also analyzed using SEM/EDS technique. Typical SEM microimages of powder samples of the two minerals are shown in Fig. 5a and b, respectively. The characteristic hexagonal plates and the layered nature of kaolinite structure are evident in Fig. 5a. The heterogeneous nature of magnesite surface is seen from Fig. 5b, which also shows the magnesite crystals to possess a rod-like morphology. The EDS analysis (reported as mole percentages) revealed that natural kaolinite was composed of 64.2% $SiO_2$, 33.5% $Al_2O_3$, and minor quantities of $K_2O$ and CaO, probably originating from small amounts of associated non-kaolinitic mineral impurities. Natural magnesite samples were composed of 29.3% $CO_2$, 22.6% MgO, 27.9% $SiO_2$, 17.8% $Al_2O_3$, and 2.4% CaO. The values represent an average of five measurements that were taken at different points of the mineral surface. The maximum deviation of the major components from the average value in the measurements performed on natural kaolinite was less than 10%, whereas the same deviation in the case of magnesite amounted in some cases to

**Table 2.** Assignments of the bands appearing in the DRIFT spectrum of natural magnesite.

| Band Position ($cm^{-1}$) | Vibration Assignment |
|---|---|
| 3700[a] | Inner surface −OH stretching vibration |
| 3620[a] | Inner −OH stretching vibration |
| 1461 | Asymmetric stretching |
| 884 | Out-of-plane bending |
| 748 | In-plane-bending |
| 2539 | Combination modes ($\nu_1 + \nu_3$) |
| 1824 | Combination modes ($\nu_1 + \nu_4$) |

a: Bands arising from the presence of some kaolinite as an impurity in the natural magnesite sample.

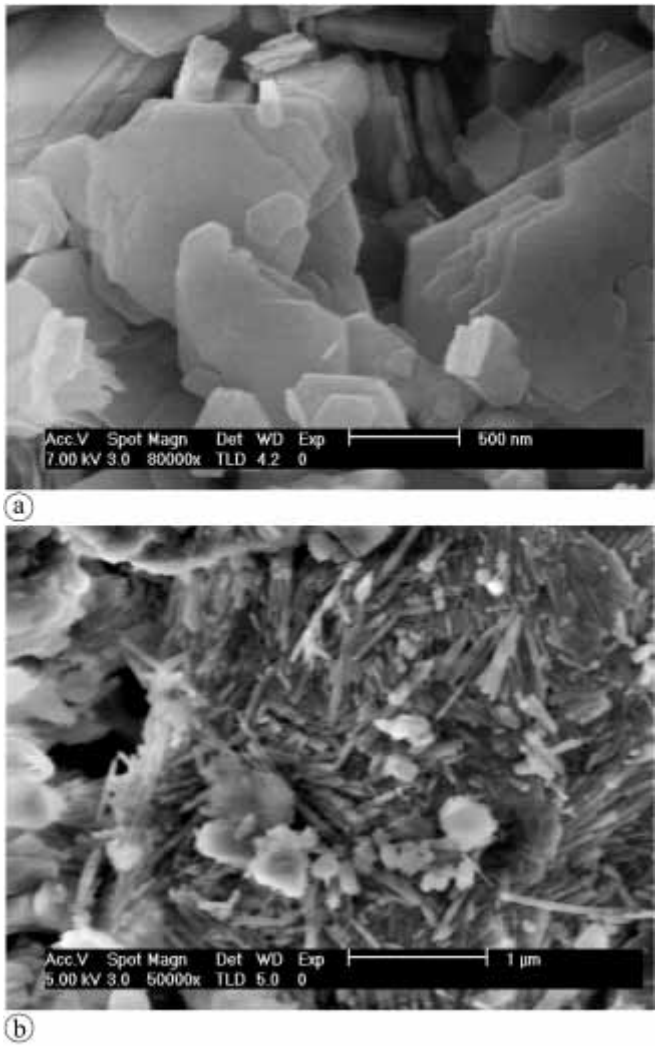


**Fig. 5.** SEM microimages of the surfaces of: (**a**) natural kaolinite, (**b**) natural magnesite.

about 50% verifying the heterogeneous nature of the magnesite surface.

## Characterization of the $Sr^{2+}$-sorbed minerals

XPS is an inherent surface sensitive technique that has been applied in various studies for qualitative and quantitative characterization of sorption [24–30]. In this work, the XPS measurements were used to elucidate the elemental contents of the natural and Sr-sorbed mineral samples. Typical spectra for kaolinite and magnesite minerals before and after $Sr^{2+}$ sorption are given in Fig. 6a and b, respectively. The XPS data were corrected using the corresponding sensitivity factors of the elements, and then the resulting amounts were normalized to the sum of Al and Si amounts. Here it was assumed that the quantities of Al and Si did not change in the course of the sorption process, as it was unlikely for such skeletal elements to take part in any exchange process. In order to verify this, blank experiments were performed in which kaolinite was mixed with de-ionized water for the same period applied in the sorption experiments. The results of the AAS measurements indicated that the concentration of both of Al and Si in solution are below the detection limit of the instrument (order of magnitude of ppb). The same was

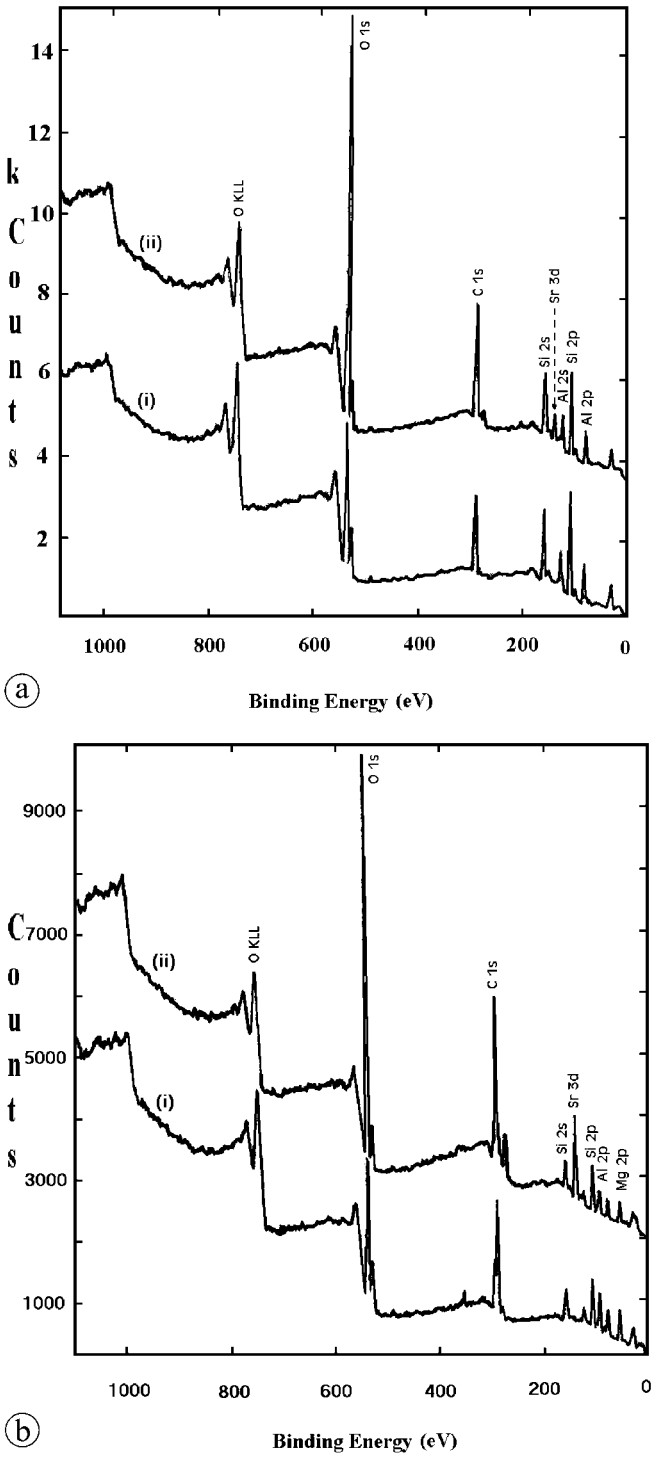


**Fig. 6.** Typical XPS spectra of: (**a**) natural kaolinite (i), and Sr-sorbed kaolinite (ii), (**b**) natural magnesite (i), and Sr-sorbed magnesite (ii).

also verified in solutions of $Sr^{2+}$ obtained following the sorption experiments.

In the case of sorption on kaolinite, the pH was in the approximate range 5.7–7.3 depending on the initial concentration of $Sr^{2+}$ solutions. This value is above the zero point of charge of kaolinite ($\sim 3.5$), the thing that ensures that the kaolinite surface is negatively charged. In general, the pH increased as the initial concentration of $Sr^{2+}$ in solution decreased. The ratios of all the detected elements in the natural samples of kaolinite and magnesite (excluding C and O) prior to and following $Sr^{2+}$ sorption are given in Tables 3

**Table 3.** The percentage elemental composition of natural kaolinite before and after $Sr^{2+}$ sorption and the element/(Al+Si) ratios calculated using the XPS data.

| | % Composition | | Element/(Al+Si) | |
|---|---|---|---|---|
| Element | Kaolinite | Sr-Kaolinite | Kaolinite | Sr-Kaolinite |
| Al+Si | 97.63 | 95.41 | 1.000 | 1.000 |
| Ca | 1.49 | N.D. | 0.015 | 0.000 |
| K | 0.88 | N.D. | 0.009 | 0.000 |
| Sr | 0.00 | 4.59 | 0.000 | 0.048 |

N.D.: not detected.

**Table 4.** The percentage elemental composition of natural magnesite before and after $Sr^{2+}$ sorption and the element/(Al+Si) ratios calculated using the XPS data.

| | % Composition | | Element/(Al+Si) | |
|---|---|---|---|---|
| Element | Magnesite | Sr-Magnesite | Magnesite | Sr-Magnesite |
| Al+Si | 69.59 | 71.11 | 1.000 | 1.000 |
| Mg | 27.32 | 18.12 | 0.393 | 0.255 |
| Ca | 3.09 | N.D. | 0.044 | 0.000 |
| Sr | 0.00 | 10.77 | 0.000 | 0.151 |

N.D.: not detected.

and 4, respectively. It is evident from the tables that the enrichment of $Sr^{2+}$ on natural kaolinite is accompanied with depletion in the amounts of $K^+$ and $Ca^{2+}$ initially present in the clay structure.

Similarly, the uptake of $Sr^{2+}$ by natural magnesite leads to a decrease in the amounts of $Mg^{2+}$ and $Ca^{2+}$. The variation in bulk concentration of K, Ca, and Mg was verified using AES measurements. The concentration of these elements was measured in $Sr^{2+}$-solutions prior to and following the sorption experiments. At the start of the experiments, the concentration of these elements was much below 1 ppm, resulting from the fact that de-ionized water was used in preparing the solutions of $Sr^{2+}$. The AES measurements of these elements after sorption showed an increase in their concentration, indicating that an ion-exchange took place between them and the $Sr^{2+}$ fixed by the clay.

Comparing the amounts of $Sr^{2+}$ scavenged by natural kaolinite and natural magnesite it is clear that the latter is more effective in $Sr^{2+}$ fixation. EDS mapping results of the Sr-sorbed kaolinite and magnesite samples are given in Figs. 7 and 8, respectively. The maps were recorded at a magnification of 500×, corresponding to an approximate area of $200 \times 200\ \mu m^2$. Comparing the image of Sr to those of Al and Si (Fig. 7) it can be seen that Sr seems to be "homogeneously" distributed on kaolinite surface. Here it must be noted that as far as EDS analysis of Sr on aluminosilicates is concerned, that analysis must be based on the *K* line of Sr as the *L* line seemed to overlap with the *K* line of Si which possesses a close energy. EDS mapping results of Sr-sorbed natural magnesite surface (Fig. 8) revealed the heterogeneous nature of the mineral. According to images, Sr seems to be more associated with regions richer in Mg, indicating that the magnesite regions of the natural mineral are more effective in Sr fixation than the kaolinite constituents within the same mineral.

DRIFT spectra of the Sr-sorbed kaolinite revealed that Sr sorption did not cause any change in the various stretching and bending vibrations of the active modes of the natural sample given in Fig. 3. The XRPD studies on natural and Sr-sorbed kaolinite showed also that the structure of the clay

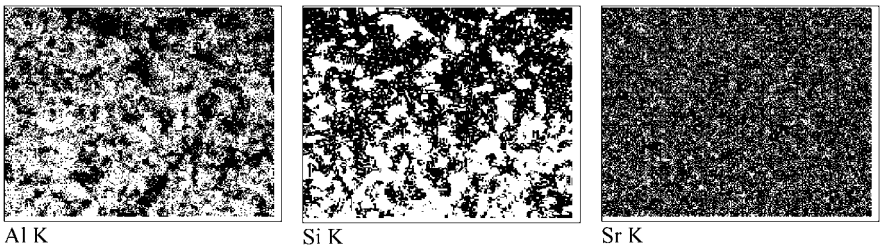


**Fig. 7.** EDS mapping of Al, Si, and Sr on the surface of natural kaolinite.

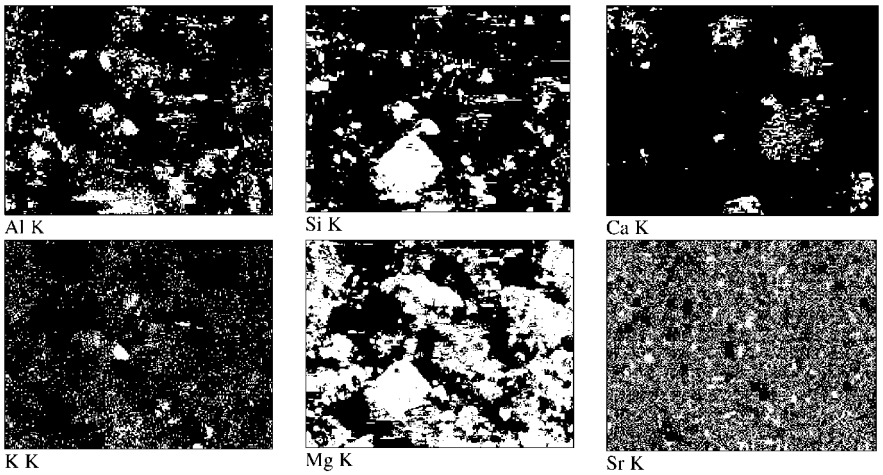


**Fig. 8.** EDS mapping of Al, Si, Ca, K, Mg, and Sr on the surface of natural magnesite.

was retained upon sorption. The fact that the XRPD peak intensities, peak shapes, and peak positions – which reflect the extent of crystallinity of the clay – along the primary 001 and 002 planes in the clay matrix were almost unaffected, is indicative that sorption has taken place on the surface and edge positions of kaolinite. This suggests that the interlayer positions of the clay were not involved in $Sr^{2+}$ fixation due to the relatively stronger binding forces among the kaolinite sheets compared to other clays like montmorillonite, where interlayer sites are much more effective in sorption than the outer sites. In order to examine the effect of expanding the interlayer space of kaolinite on the amount of adsorbed $Sr^{2+}$, the clay was intercalated with dimethylsulfoxide, DMSO ($(CH_3)_2SO$). Intercalation of DMSO in kaolinite provides a method for the incorporation of alkali and alkaline metal salts into the kaolinite structure by replacement of DMSO [31]. DMSO molecules are bound into the kaolinite structure by hydrogen bonding of the S=O to the gibbsite-like hydroxyls and by a coordination of the sulfur to the oxygens of the siloxane surface [31] . Intercalation of DMSO within the kaolinite lamellae caused a change in position of the primary 001 and 002 reflections to higher $d_{hkl}$ values. Fig. 1b shows the increase of $d_{001}$ from 0.72 nm to 1.13 nm The figure shows also that DMSO molecules were readily removed from kaolinite upon the exposure of the clay to $Sr^{2+}$ solutions as indicated by the re-appearance of the XRPD reflections at their original spacing. The bulk analysis of the $Sr^{2+}$ solutions using AES at the end of the mixing period indicated that the difference in the $Sr^{2+}$ concentration between the solutions that were exposed to natural kaolinite and those exposed to DMSO-intercalated kaolinite was small. In both cases, the percentage sorption was calculated to be around 39, 56, and 62% for solutions with initial $Sr^{2+}$ concentration of $1.0 \times 10^{-2}$, $1.0 \times 10^{-4}$, and $1.0 \times 10^{-6}$ M, respectively. This can be probably explained by assuming that $Sr^{2+}$ which displaced DMSO in the interlayer region of kaolinite have experienced a fast sorption step, which lead to displacing DMSO molecules, followed by a desorption step during the later stages of mixing, leading to the removal of most of $Sr^{2+}$ ions from the interlayer region. The forces of interaction during the sorption step could be weak van der Waals type forces, the thing that might have facilitated desorption under the effect of mixing. The interlayer region of kaolinite is known to be tightly packed, and unless there is an isomorphous substitution in this region, no permanent negative charge will develop on the internal surfaces like it is the case in expandable clays such as montmorillonite. The presence of a negative charge on accessible sites is essential for a stable binding of positive cations like $Sr^{2+}$.

The XPRD characterization of magnesite before and after $Sr^{2+}$ sorption has also shown that the matrix of the mineral did not undergo structural changes at different loadings. Fig. 2b shows the XRPD diagram of Sr-loaded natural magnesite prepared at an initial $Sr^{2+}$ concentration of $1.0 \times 10^{-2}$ M. The same observation is evident also from the DRIFT characterization, which showed that the vibrational bands shown in Fig. 4 were all unaffected. As previously mentioned, no pH adjustment was made and the pH ranged from 8.2–7.6 during the mixing process of $Sr^{2+}$ ions with natural magnesite.

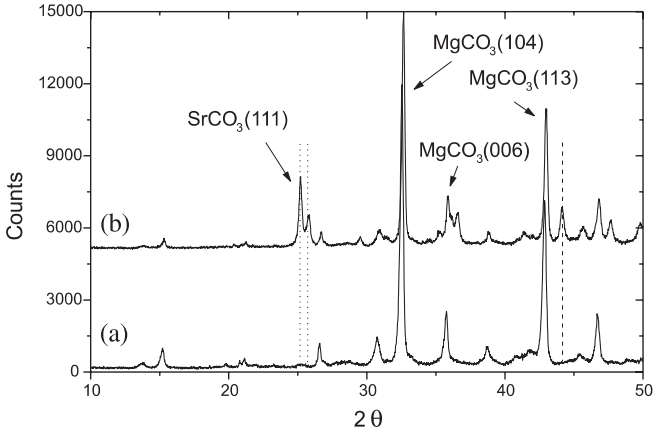


**Fig. 9.** XRPD diagram of: (a) pure $MgCO_3$, (b) Sr-sorbed $MgCO_3$.

The sorption of $Sr^{2+}$ ions was also studied on pure $MgCO_3$ samples. Unlike the case in natural magnesite, the XRPD analysis of the Sr-sorbed samples revealed the formation of strontianite ($SrCO_3$) as a coprecipitate on the $MgCO_3$ samples treated with an initial $Sr^{2+}$ concentration of $1.0 \times 10^{-2}$ M (Fig. 9). Here also there was no pH control but the pH in these experiments ranged from 10.5–8.3, higher than the range reported above for natural magnesite, thus indicating that the medium was richer in $CO_3^{2-}$ ions. In both cases, the decrease in the pH at the end of mixing could plausibly be caused by the removal of carbonate ions from the medium either upon formation of $SrCO_3$ or the re-precipitation of $CaCO_3$. It is not clear what is the exact reason that makes natural magnesite less soluble than $MgCO_3$, but it might be considered that the presence of impurities within magnesite, in particular near the surface, could have kinetically inhibited its solubility. In a study on calcite [32], it was reported that some metal ions encountered within the surface of this mineral at even small concentration could lead to inhibiting the solubility of the mineral. According to the same study, in solid–liquid interaction, barriers against mixing might develop, leading to kinetic stabilization of the reaction far from thermodynamic stabilization.

The formation of strontianite was characterized by an enhanced ability of $MgCO_3$ towards the uptake of $Sr^{2+}$ compared to a much lower ability at the lower $Sr^{2+}$ concentrations of $1.0 \times 10^{-4}$ and $1.0 \times 10^{-6}$ M, for which no strontianite formation was detected. The EDS results for the pure $MgCO_3$ samples prior to and following $Sr^{2+}$ sorption are given in Table 5. The data were collected from 5 different

**Table 5.** The chemical analysis (% Mol) of pure $MgCO_3$ and Sr-sorbed $MgCO_3$ obtained from the EDS analysis at different initial concentration of $Sr^{2+}$.

| Constituent | $MgCO_3$ | Sr-sorbed $MgCO_3$ | | |
|---|---|---|---|---|
| | | $1.0 \times 10^{-6}$ M | $1.0 \times 10^{-4}$ M | $1.0 \times 10^{-2}$ M |
| $CO_2$ | 57.8 | 58.7 | 58.4 | 59.6 |
| MgO | 40.3 | 39.6 | 39.2 | 35.3 |
| CaO | 0.8 | 0.7 | 0.7 | 0.6 |
| Others | 1.1 | 0.9 | 0.6 | 0.1 |
| SrO | – | N.D. | 1.1 | 4.4 |

N.D.: not detected.

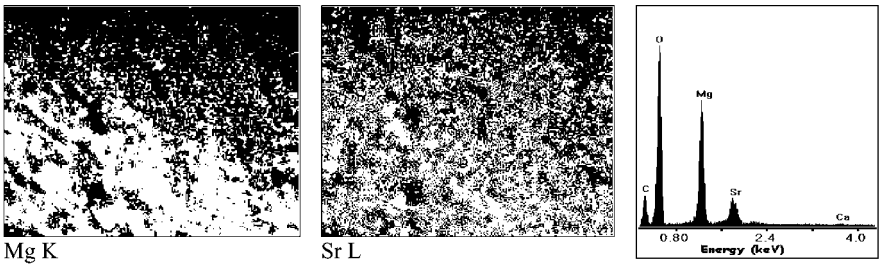


**Fig. 10.** EDS mapping of Mg and Sr on the surface of Sr-sorbed $MgCO_3$. A typical EDS spectrum is also shown.

points and the values given in the table represent the average with maximum deviations from the average values of 2.9%, 4.2%, and 8.7% for $CO_2$, MgO and SrO, respectively. The EDS mapping of Mg and Sr on $MgCO_3$ is given in Fig. 10. The figure shows Sr to be spread all over the surface but at higher concentrations in certain regions than the others. Spot analysis of the brighter regions on Sr map verified that the larger concentration of the ion was associated with the presence of strontianite.

## Sorption mechanisms of $Sr^{2+}$ ions

### Sorption on natural kaolinite

According to the XPS findings, $K^+$ and $Ca^{2+}$, initially present in natural kaolinite, were depleted upon sorption of $Sr^{2+}$ ions. Such ions are normally not encountered in the structure of pure kaolinite, and it seems that they were associated with an impurity that exists in minor quantity in the natural clay, or were initially attached to vacant sites on the clay surface. The removal of these elements upon fixation of $Sr^{2+}$ is indicative of the contribution of ion exchange mechanism to the sorption process. Furthermore, the fact that the total quantities of both of $K^+$ and $Ca^{2+}$ were only one half the quantity of sorbed $Sr^{2+}$ (see Table 3), points to the fact that ion exchange is not the sole mechanism of uptake.

As outlined above, the XRPD characterization of natural and Sr-loaded kaolinite showed no change in the basic reflections of the clay upon sorption. Moreover, expanding the interlayer space of kaolinite by intercalation of DMSO, did not lead to a significant enhancement of $Sr^{2+}$ uptake by the clay. This can be an indication that sorption of $Sr^{2+}$ on kaolinite occurs mainly on the outer surface and edges of kaolinite. During the sorption experiments on this clay, pH was in the approximate range 5.7–7.3 depending on the initial concentration of $Sr^{2+}$ solutions. This pH range is above the zero point of charge of kaolinite ($\sim 3.5$), the thing that ensures that the kaolinite surface is negatively charged. Hence, in addition to ion-exchange discussed above, another possible mechanism of $Sr^{2+}$ sorption might be operating through interactions with the $AlO^-$ and $SiO^-$ sites created as a result of the deprotonation of the acidic hydroxyl groups. The extent of such protonation is pH-dependent and is referred to as 'hydrolytic adsorption' that can be described by the following Eq. (1):

$$\text{surface}-\text{OH} + \text{Sr}^{2+} \rightarrow \text{surface}-\text{O}-\text{Sr}^{+} + \text{H}^{+} . \quad (1)$$

It is reported that the external charge on kaolinite surface can be attributed to silanol groups as well as amphoteric aluminol groups at the crystal edges which deprotonate yielding $SiO^-$ and $AlO^-$ surface complexes at moderate and high pH values [33]. Hence, in the absence of impurities that might give rise to ion-exchange in natural kaolinite, hydrolytic sorption will be the primary mechanism that will determine the cation exchange capacity of pure kaolinite.

### Sorption on natural magnesite and pure $MgCO_3$

The surface of carbonate minerals possesses a dynamic nature and, as a result, the fixation of 'foreign' ions can take place *via* a variety of mechanisms. These mechanisms includes ion exchange, burial of the ions within the lattice of carbonate upon recrystallization, binding of the ions to coordinative unsaturated carbonate groups (or specie) at the surface of the mineral, precipitation in a distinct phase as metal carbonate, metal hydroxide, or both, and solid state diffusion (negligible for low residence times of less than 100 years [34]). The nature of solution medium (concentration, pH, and temperature) and the type of surface speciation taking place at the solid–liquid interface will determine the type of fixation. According to our results, in the case of natural magnesite, in the absence of any $SrCO_3$ formation (as revealed by XRPD findings) and based on the comparison of the quantity of fixed $Sr^{2+}$ to that of depleted $Mg^{2+}$ (as obtained from XPS data; Table 4), ion exchange seems to be the primary process of sorption. Similar observations were reported for $Sr^{2+}$ sorption on calcite [15, 35, 36]. The fact that the $Sr^{2+}$ neighboring structural environment in Sr-sorbed calcite was similar to calcite rather than to strontianite was used as an evidence that the uptake of $Sr^{2+}$ ions occurred *via* an ion exchange mechanism [36].

On the other hand, in the case of $MgCO_3$, fixation seems to be dominated by $SrCO_3$ formation, the thing possibly stemming from the higher concentration of carbonate in the reaction medium as discussed previously. Other sorption mechanisms could have done some contribution to the amount of scavenged $Sr^{2+}$ ions, but their role seems to be insignificant. It is reported that precipitation mechanism leads to enhancement of removal of ions from solution and greatly immobilize these ions by 'freezing' them in the host mineral structure [37], the thing inline with our results which revealed a higher ability of $MgCO_3$ to fix $Sr^{2+}$ compared to natural magnesite.

## Conclusion

Natural kaolinite and magnesite used in this study were of heterogeneous nature. Based on XPS findings, natural magnesite showed higher sorption capacity compared to natural kaolinite. The fact that the structure of kaolinite was retained upon $Sr^{2+}$ uptake indicates that surface and edge sites

are more effective in sorption. The EDS mapping of kaolinite surface indicated that $Sr^{2+}$ was equally distributed on that surface. The absence of any precipitate formation in the case of $Sr^{2+}$ fixation by natural magnesite, and based on XPS quantification analysis, the uptake mechanism on this mineral seems to occur primarily *via* ion exchange. The high depletion of $Mg^{2+}$ upon $Sr^{2+}$ sorption supported this observation, the thing also clear from the EDS maps which showed that Sr was localized in a larger extents at regions richer in Mg. Unlike the case of natural magnesite, the sorption mechanism of $Sr^{2+}$ by pure $MgCO_3$ involved a $SrCO_3$ precipitate formation, the thing referred to the higher pH of the aqueous $MgCO_3$ medium. Precipitate formation lead to an enhanced removal of $Sr^{2+}$ compared to the situations where $Sr^{2+}$ is removed by an ion-exchange type mechanism.

*Acknowledgment.* The authors would like to thank Dr. K. Hallam at the Interface Analysis Centre/University of Bristol for his help in the XPS measurements. Ms. Duygu Oguz and Mr. Gokhan Erdogan at the Center of Material Research/Izmir Institute of Technology for their help in the SEM/EDS measurements.

## References

1. Lieser, K. H.: Radionuclides in the geosphere: sources, mobility, reactions in natural waters and interactions with solids. Radiochim. Acta **70**/**71**, 355 (1995).
2. Hsu, C., Liu, D., Chuang, C.: Equilibrium and kinetic sorption behaviors of cesium and strontium in soils. Appl. Radiat. Isotope **45**, 981 (1994).
3. Wang; X., Chen; Y., Wu, Y.: Sorption and desorption of radiostrontium on powdered bentonite: Effect of pH and fulvic acid. J. Radioanal. Nucl. Chem. **261**, 497 (2004).
4. Khan, S. A.: Sorption of the long-lived radionuclides cesium-134, strontium-85 and cobalt-60 on bentonite, J. Radioanal Nucl. Chem. **258**, 3 (2003).
5. Iwaida, T., Nagasaki, S., Tanaka, S.: Sorption study of strontium onto hydrated cement phases using a sequential desorption method. Radiochim. Acta **88**, 483 (2000).
6. Khan, S. A., Rehman, R., Khan, M. A.: Sorption of strontium on Bentonite. Waste Management **15**, 641 (1995).
7. Liang, T.: The influence of cation concentration on the sorption of strontium on mordenite. Appl. Radiat. Isotopes **51**, 527 (1999).
8. Karasyova, O. N., Ivanova, L. I., Lakshtanov, L. Z., Lövgren, L.: Strontium sorption on hematite at elevated temperatures. J. Colloid Interf. Sci. **220**, 419 (1999).
9. Bors, J., Dultz, St., Riebe, B.: Retention of radionuclides by organophilic bentonite. Eng. Geol. **54**, 195 (1999).
10. Eriksen, T. E., Jansson, M., Molera, M.: Sorption effects on cation diffusion in compacted bentonite. Eng. Geol. **54**, 231 (1999).
11. Zhu, C.: Estimation of surface precipitation constants for sorption of divalent metals onto hydrous ferric oxide and calcite. Chem. Geol. **188**, 23 (2002).
12. Nakashima, Y.: Diffusivity measurement of heavy ions in Wyoming montmorillonite gels by X-ray computed tomography. J. Contam. Hydrol. **61**, 147 (2003).
13. Juang, R., Lin, S., Wang, T.: Removal of metal ions from the complexed solutions in fixed bed using a strong-acid ion exchange resin. Chemosphere **53**, 1221 (2003).
14. Sahai, N., Carroll, S. A., Roberts, S., O'Day, P. A.: X-Ray absorption spectroscopy of strontium(II) coordination: II. sorption and precipitation at kaolinite, amorphous silica, and goethite surfaces. J. Colloid Interf. Sci. **222**, 198 (2000).
15. Parkman, R. H., Charnock, J. M., Livens, F. R., Vaughan, D. J.: A study of the interaction of strontium ions in aqueous solution with the surfaces of calcite and kaolinite. Geochim. Cosmochim. Acta **62**, 1481 (1998).
16. Nordstrom, D. K., McNutt, R. H., Puigdomènech, I., Smellie, J. A. T., Wolf, M.: Ground water chemistry and geochemical modeling of water–rock interactions at the Osamu Utsumi mine and the Morro do Ferro analogue study sites, Poços de Caldas, Minas Gerais, Brazil. J. Geochem. Explor. **45**, 249 (1992).
17. Cole, T., Bidoglio, G., Soupioni, M., O'Gorman, M., Gibson, N.: Diffusion mechanisms of multiple strontium species in clay. Geochim. Cosmochim. Acta **64**, 385 (2000).
18. Bergaya, F., Vayer, M.: CEC of clays: Measurement by adsorption of a copper ethylenediamine complex. Appl. Clay Sci. **12**, 275 (1997).
19. Baes Jr., C. F., Mesmer, R. E.: *The Hydrolysis of Cations*. John Wiley & Sons Inc. (1976).
20. Patakfalvi, R., Oszko, A., Dekany I.: Synthesis and characterization of silver nanoparticle/kaolinite composites. Colloid Surface A **220**, 45 (2003).
21. Wilson, M. J.: *Clay Mineralogy: Spectroscopic and Chemical Determination Methods*. Chapman & Hall, London (1994).
22. Suraj, G., Iyer, C. S. P., Rugmini, S., Lalithambika, M.: The effect of microionization on kaolinites and their sorption behavior. Appl. Clay Sci. **12**, 111 (1997).
23. Böttcher, M. E., Gehlken, P., Steele, D. F.: Characterization of inorganic and biogenic magnesian calcites by Fourier Transform infrared spectroscopy. Solid State Ionics **101**–**103**, 1379 (1997).
24. Shahwan, T., Suzer, S., Erten, H. N.: Sorption studies of $Cs^{+}$ and $Ba^{2+}$ cations on magnesite. Appl. Radiat. Isotopes **49**, 915 (1998).
25. Ning, X., Hochella Jr., M. F., Brown Jr., G. E., Parks, G. A.: Co(II) sorption at the calcite–water interface: I. X-ray photoelectron spectroscopic study. Geochim. Cosmochim. Acta **60**, 2801 (1996)
26. Drot, R., Simoni, E., Alnot, M., Ehrhardt, J. J.: Structural environment of uranium(VI) and europium(III) species sorbed onto phosphate surfaces: XPS and optical spectroscopy studies. J. Colloid Interf. Sci. **205**, 410 (1998).
27. Dutta, N. C., Iwasaki, T., Ebina, T., Hayashi, H.: A combined X-ray photoelectron and auger electron spectroscopic study of cesium in variable-charge montmorillonites. J. Colloid Interf. Sci. **216**, 161 (1999)
28. Merdy, P., Guillon, E., Aplincourt, M., Dumonceau, J., Vezin, H.: Copper sorption on a straw lignin: experiments and EPR characterization. J. Colloid Interf. Sci. **245**, 24 (2002).
29. García-Sánchez, A., Álvarez-Ayuso, E.: Sorption of Zn, Cd and Cr on calcite. Application to purification of industrial wastewaters. Miner. Eng. **15**, 539 (2002).
30. Lomenech, C., Simoni, E., Drot, R., Ehrhardt, J. J., Mielczarski, J.: Sorption of uranium(VI) species on zircon: structural investigation of the solid/solution interface. J. Colloid Interf. Sci. **261**, 221 (2003).
31. Frost, R. L., Kristof, J., Paroz, G. N., Kloprogge, J. T.: Molecular structure of dimethyl sulfoxide intercalated kaolinite. J. Phys. Chem B **102**, 8519 (1998).
32. Hay, M. B., Workman, R. K. Manne, S.: Mechanisms of metal ion sorption on calcite: composition mapping by lateral force microscopy. Langmuir **19**, 3727 (2003).
33. Coppin, F., Berger, G., Bauer, A., Castet, S., Loubet, M.: Sorption of lanthanides on smectite and kaolinite. Chem. Geol. **182**, 57 (2002).
34. Hoffman, U., Stipp, S. L. S.: The behavior of $Ni^{2+}$ on calcite surface. Geochim. Cosmochim. Acta **65**, 4131 (2001).
35. Zachara, J. M., Cowan, C. E., Resch, C. T.: Sorption of divalent metals on calcite. Geochim. Cosmochim. Acta **55**, 1549 (1991).
36. Pingitore Jr., N. E., Lytle, F. W., Davies, B. M., Eastman, M. P., Eller, P. G., Larson, E. M.: Mode of incorporation of $Sr^{2+}$ in calcite: Determination by X-ray absorption spectroscopy. Geochim. Cosmochim. Acta **56**, 1531 (1992).
37. Wang, Y., Xu, H.: Prediction of trace metal partitioning between minerals and aqueous solutions: a linear free energy correlation approach. Geochim. Cosmochim. Acta **65**, 1529 (2001).